universe

MDPI

Article

A Post-Newtonian Gravitomagnetic Effect on the Orbital Motion of a Test Particle around Its Primary Induced by the Spin of a Distant Third Body

Lorenzo Iorio

Ministero dell'Istruzione, dell'Università e della Ricerca (M.I.U.R.)-Istruzione, Viale Unità di Italia 68, 70125 Bari (BA), Italy; lorenzo.iorio@libero.it

Received: 4 March 2019; Accepted: 28 March 2019; Published: 31 March 2019



Abstract: We study a general relativistic gravitomagnetic 3-body effect induced by the spin angular momentum $\boldsymbol{S}_\mathrm{X}$ of a rotating mass M_X orbited at distance r_X by a local gravitationally bound restricted two-body system $\mathcal{S}$ of size $r \ll r_\mathrm{X}$ consisting of a test particle revolving around a massive body M. At the lowest post-Newtonian order, we analytically work out the doubly averaged rates of change of the Keplerian orbital elements of the test particle by finding non-vanishing long-term effects for the inclination I, the node Ω and the pericenter ω. Such theoretical results are confirmed by a numerical integration of the equations of motion for a fictitious 3-body system. We numerically calculate the magnitudes of the post-Newtonian gravitomagnetic 3-body precessions for some astronomical scenarios in our solar system. For putative man-made orbiters of the natural moons Enceladus and Europa in the external fields of Saturn and Jupiter, the relativistic precessions due to the angular momenta of the gaseous giant planets can be as large as $\simeq 10 - 50$ milliarcseconds per year $\left(\mathrm{mas\ year}^{-1}\right)$. A preliminary numerical simulation shows that, for certain orbital configurations of a hypothetical Europa orbiter, its range-rate signal $\Delta\dot{\rho}$ can become larger than the current Doppler accuracy of the existing spacecraft Juno at Jupiter, i.e., $\sigma_{\dot{\rho}} = 0.015\ \mathrm{mm\ s}^{-1}$, after 1 d. The effects induced by the Sun's angular momentum on artificial probes of Mercury and the Earth are at the level of $\simeq 1 - 0.1$ microarcseconds per year $\left(\mu\mathrm{as\ year}^{-1}\right)$.

Keywords: general relativity and gravitation; experimental studies of gravity; experimental tests of gravitational theories; satellite orbits

1. Introduction

Let us consider a local gravitationally bound restricted two-body system $\mathcal{S}$ composed by a test particle completing a full orbital revolution around a planet of mass M at distance r in a time interval P_b, and a distant 3rd body X with mass $M_\mathrm{X} \gg M$ and proper spin $\boldsymbol{S}_\mathrm{X}$ around which $\mathcal{S}$ revolves at distance $r_\mathrm{X} \gg r$ with orbital period P_b^X. In general, M may be endowed with its own Newtonian and post-Newtonian (pN) mass and spin multipole moments [1,2] affecting the satellite's motion with known [3,4] and less known [5–7] Newtonian and pN orbital effects like the classical oblateness-driven orbital precessions, the gravitoelectric Einstein pericentre shift, the gravitomagnetic Lense-Thirring effect, etc. Let us consider a kinematically rotating and dynamically non-rotating coordinate system $\mathcal{K}$ [8–10] attached to M in geodesic motion through the external spacetime deformed by the mass-energy currents of X, assumed stationary in a kinematically and dynamically non-rotating coordinate system $\mathcal{K}_\mathrm{X}$ whose axes point towards the distant quasars [8–10]. The planetocentric motion of the test particle referred to $\mathcal{K}$ is further affected by two peculiar pN 3-body effects: the time-honored De Sitter precession due to solely the mass M_X [11–13], and a gravitomagnetic shift due to $\boldsymbol{S}_\mathrm{X}$ which, to our knowledge, has never been explicitly and clearly calculated in the literature, if it had ever been. Our purpose is to analytically work out the latter effect at the lowest pN order without any a-priori simplifying assumptions concerning both the orbital configurations of the planetocentric satellite's motion and the trajectory of the planet-satellite system $\mathcal{S}$ in the external field of X, and for an arbitrary orientation of $\boldsymbol{S}_\mathrm{X}$ in space. For the previous, approximate calculation restricted to the orbital

angular momentum of the Moon orbiting the Earth in the field of the rotating Sun, see Gill et al. [14] (Section 3.3.3).

The plan of the paper is as follows. In Section 2, we analytically work out the long-term rates of change of the Keplerian orbital elements of the test particle. Section 3 is devoted to the application of the obtained results to some astronomical scenarios in our solar system. We summarize our results and offer our conclusions in Section 4. For the benefit of the reader, Appendix A contains a list of the definitions of the symbols used in the paper, while their numerical values and tables are collected in Appendix B.

2. The Doubly Averaged Satellite's Orbital Precessions

In the weak-field and slow-motion approximation of general relativity, the gravitomagnetic 3-body potential induced by the angular momentum $\boldsymbol{S}_{\rm X}$ of the external spinning object X on the planetary satellite is

$$U_{\rm GM} = \frac{G}{c^2 r_{\rm X}^3}\boldsymbol{S}_{\rm X}\cdot\left[-\boldsymbol{L}+3\left(\boldsymbol{L}\cdot\hat{\boldsymbol{r}}_{\rm X}\right)\hat{\boldsymbol{r}}_{\rm X}\right]. \tag{1}$$

In Equation (1), G, c are the Newtonian constant of gravitation and the speed of light in vacuum, respectively, while $\boldsymbol{L}$ being the angular momentum per unit mass of the test particle's orbital motion around M. Equation (1) comes from Equation (2.19) of Barker & O'Connell [15] (p. 155) for the interaction potential energy $V_{S1,S2}$ of two spins $\boldsymbol{S}^{(1)}$, $\boldsymbol{S}^{(2)}$ of masses m_1, m_2 separated by a distance r and moving with relative speed v in the limit $m_2\equiv M_{\rm X}\gg m_1\equiv M$, and by assuming that the spin $\boldsymbol{S}^{(1)}$ is the orbital angular momentum of the planetocentric satellite's motion while $\boldsymbol{S}^{(2)}$ is the spin angular momentum $\boldsymbol{S}_{\rm X}$ of the distant 3rd body X. Thus, r in Equation (2.19) of Barker & O'Connell [15] (p. 155) has to be identified with $r_{\rm X}$, and $\boldsymbol{r}\times\boldsymbol{P}$ is nothing but the orbital angular momentum $\boldsymbol{r}_{\rm X}\times M\boldsymbol{v}_{\rm X}$ of the motion of $\mathcal{S}$ around $M_{\rm X}$. It is interesting to note that, with the same identifications, V_{S1} and V_{S2} of Equations (2.17) and (2.18) in Barker & O'Connell [15] (p. 155) yield the gravitoelectric De Sitter orbital precession for the planetocentric motion of the satellite and the gravitomagnetic Lense-Thirring effect for the X-centric orbit of M, respectively.

The velocity-dependent perturbing potential $U_{\rm pert}$ to be inserted into the Lagrange planetary equations [10,16] for the rates of change of the nonosculating [10,17] Keplerian orbital elements of the test particle, obtained by doubly averaging Equation (1) with respect to $P_{\rm b}$, $P_{\rm b}^{\rm X}$ for arbitrary orbital configurations of both the external body X and the test particle and for a generic orientation of $\boldsymbol{S}_{\rm X}$ in space, is

$$U_{\rm pert} = \overline{\overline{U}}_{\rm GM} = -\frac{GS_{\rm X}n_{\rm b}a^2\sqrt{1-e^2}}{2c^2a_{\rm X}^3\left(1-e_{\rm X}^2\right)^{3/2}}\mathcal{U}, \tag{2}$$

with

$$\begin{aligned}\mathcal{U} = {}& \cos I\left\{2\hat{S}_z-3\sin I_{\rm X}\left[\hat{S}_z\sin I_{\rm X}+\cos I_{\rm X}\left(\hat{S}_y\cos\Omega_{\rm X}-\hat{S}_x\sin\Omega_{\rm X}\right)\right]\right\}+\\ &+\frac{\sin I}{2}\left\{2\hat{S}_y\cos\Omega-2\hat{S}_x\sin\Omega+3\cos\left(\Omega-\Omega_{\rm X}\right)\left[\hat{S}_z\sin 2I_{\rm X}+\right.\right.\\ &\left.\left.+\,2\sin^2 I_{\rm X}\left(-\hat{S}_y\cos\Omega_{\rm X}+\hat{S}_x\sin\Omega_{\rm X}\right)\right]\right\}.\end{aligned} \tag{3}$$

In Equations (2) and (3), a, e, I, $a_{\rm X}$, $e_{\rm X}$, $I_{\rm X}$ are the semimajor axes, the eccentricities and the inclinations of the orbits of the test particle and of $\mathcal{S}$, respectively, while $n_{\rm b}$ is the Keplerian orbital motion of the satellite's planetary motion about M. Equations (2) and (3) were obtained in two steps. First, $U_{\rm GM}$ of Equation (1) was evaluated onto the unperturbed ellipse of the planetocentric satellite motion through the standard Keplerian formulas of the restricted two-body problem (see, e.g., Equations (3.40a) to (3.41c) of Poisson & Will [4]). Then, it was averaged over one orbital period $P_{\rm b}$ to the first order in the disturbing potential by using just the Keplerian part of Equation (3.66) of Poisson & Will [4] for df/dt, where f is the true anomaly. Then, the resulting averaged potential $\overline{U}_{\rm GM}$ was, in turn, calculated onto the unperturbed Keplerian trajectory of $\mathcal{S}$ about X and averaged over $P_{\rm b}^{\rm X}$ to

the first order in the perturbation under consideration, thus finally obtaining the double average of Equations (2) and (3).

Inserting Equations (2) and (3) into the right-hand-sides of the Lagrange planetary equations allows to calculate the doubly averaged rates of change of the Keplerian orbital elements. They turn out to be

$$\dot{a} = 0, \tag{4}$$

$$\dot{e} = 0, \tag{5}$$

$$\dot{I} = -\frac{GS_{\rm X}}{2a_{\rm X}^3c^2\left(1-e_{\rm X}^2\right)^{3/2}}\mathcal{I}, \tag{6}$$

$$\dot{\Omega} = -\frac{GS_{\rm X}}{2a_{\rm X}^3c^2\left(1-e_{\rm X}^2\right)^{3/2}}\mathcal{O}, \tag{7}$$

$$\dot{\omega} = -\frac{GS_{\rm X}\csc I}{8a_{\rm X}^3c^2\left(1-e_{\rm X}^2\right)^{3/2}}\mathcal{P}. \tag{8}$$

with

$$\begin{aligned}\mathcal{I} = {} & \sin\Omega\left\{-\hat{S}_y + 3\sin I_{\rm X}\cos\Omega_{\rm X}\left[-\hat{S}_z\cos I_{\rm X} + \sin I_{\rm X}\left(\hat{S}_y\cos\Omega_{\rm X} - \hat{S}_x\sin\Omega_{\rm X}\right)\right]\right\} + \\ & + \cos\Omega\left\{-\hat{S}_x + 3\sin I_{\rm X}\sin\Omega_{\rm X}\left[\hat{S}_z\cos I_{\rm X} + \sin I_{\rm X}\left(-\hat{S}_y\cos\Omega_{\rm X} + \hat{S}_x\sin\Omega_{\rm X}\right)\right]\right\},\end{aligned} \tag{9}$$

$$\begin{aligned}\mathcal{O} = {} & 2\hat{S}_z + \hat{S}_x\cot I\sin\Omega - 3\cos I_{\rm X}\sin I_{\rm X}\left(\hat{S}_y\cos\Omega_{\rm X} - \hat{S}_x\sin\Omega_{\rm X} + \hat{S}_z\cot I\sin\Omega\sin\Omega_{\rm X}\right) - \\ & - 3\sin^2 I_{\rm X}\left[\hat{S}_z + \cot I\sin\Omega\sin\Omega_{\rm X}\left(-\hat{S}_y\cos\Omega_{\rm X} + \hat{S}_x\sin\Omega_{\rm X}\right)\right] + \\ & + \cos\Omega\cot I\left\{-\hat{S}_y + 3\sin I_{\rm X}\cos\Omega_{\rm X}\left[-\hat{S}_z\cos I_{\rm X} + \sin I_{\rm X}\left(\hat{S}_y\cos\Omega_{\rm X} - \hat{S}_x\sin\Omega_{\rm X}\right)\right]\right\},\end{aligned} \tag{10}$$

$$\begin{aligned}\mathcal{P} = {} & \hat{S}_y\left[\cos\Omega - 3\cos\left(\Omega - 2\Omega_{\rm X}\right)\right] - \hat{S}_x\left[\sin\Omega + 3\sin\left(\Omega - 2\Omega_{\rm X}\right)\right] + \\ & + 6\cos\left(\Omega - \Omega_{\rm X}\right)\left[\hat{S}_z\sin 2I_{\rm X} + \cos 2I_{\rm X}\left(\hat{S}_y\cos\Omega_{\rm X} - \hat{S}_x\sin\Omega_{\rm X}\right)\right].\end{aligned} \tag{11}$$

We remark that Equations (4) and (11) are exact in both e and $e_{\rm X}$ in the sense that the low-eccentricity approximation was not adopted in the calculation.

A more computationally cumbersome approach to obtain the same long-term rates of change of Equations (4) and (11) consists, first of all, in deriving a perturbing acceleration from Equation (1). By writing the Lagrangian per unit mass of a gravitationally bound restricted two-body system affected by a generic perturbing potential as

$$\mathcal{L} = \mathcal{L}_0 + \mathcal{L}_{\rm pert} = \frac{v^2}{2} + \frac{\mu}{r} + \mathcal{L}_{\rm pert}, \tag{12}$$

the conjugate momentum per unit mass is, by definition,

$$\boldsymbol{p} \doteq \frac{\partial\mathcal{L}}{\partial\boldsymbol{v}} = \boldsymbol{v} + \frac{\partial\mathcal{L}_{\rm pert}}{\partial\boldsymbol{v}}. \tag{13}$$

Thus,

$$\dot{\boldsymbol{p}} = \dot{\boldsymbol{v}} + \frac{d}{dt}\left(\frac{\partial \mathcal{L}_{\rm pert}}{\partial \boldsymbol{v}}\right). \tag{14}$$

The Hamiltonian per unit mass is

$$\mathcal{H} = \mathcal{H}_0 + \mathcal{H}_{\rm pert} = \frac{v^2}{2} - \frac{\mu}{r} + \mathcal{H}_{\rm pert}. \tag{15}$$

From the Hamilton equations of motion, it is

$$\dot{\boldsymbol{p}} = -\frac{\partial \mathcal{H}}{\partial \boldsymbol{r}} = -\frac{\mu}{r^3}\boldsymbol{r} - \frac{\partial \mathcal{H}_{\rm pert}}{\partial \boldsymbol{r}}. \tag{16}$$

Since $\mathcal{L}_{\rm pert} = -\mathcal{H}_{\rm pert}$, by comparing Equations (14) and (16), it turns out that the perturbing acceleration is just

$$\boldsymbol{A}^{\rm pert} = \frac{d}{dt}\left(\frac{\partial \mathcal{H}_{\rm pert}}{\partial \boldsymbol{v}}\right) - \frac{\partial \mathcal{H}_{\rm pert}}{\partial \boldsymbol{r}}. \tag{17}$$

In our specific case, since $\mathcal{H}_{\rm pert} = U_{\rm GM}$, we have

$$\boldsymbol{A}^{\rm GM} = \frac{d}{dt}\left(\frac{\partial U_{\rm GM}}{\partial \boldsymbol{v}}\right) - \frac{\partial U_{\rm GM}}{\partial \boldsymbol{r}} = \frac{2G}{c^2 r_{\rm X}^3}\boldsymbol{v} \times \left[\boldsymbol{S}_{\rm X} - 3\left(\boldsymbol{S}_{\rm X}\cdot\hat{\boldsymbol{r}}_{\rm X}\right)\hat{\boldsymbol{r}}_{\rm X}\right]. \tag{18}$$

Then, Equation (18) must be decomposed into its radial (ρ), transverse (τ) and out-of-plane (ν) components, which are

$$A_\rho^{\rm GM} = \frac{GS_{\rm X}}{c^2 r_{\rm X}^5}\left[\left(-\hat{S}_x r_{\rm X}^2 + 3\hat{S}_x x_{\rm X}^2 + 3\hat{S}_y x_{\rm X} y_{\rm X} + 3\hat{S}_z x_{\rm X} z_{\rm X}\right)\cos\Omega + \right.$$

$$\left. + \left(-\hat{S}_y r_{\rm X}^2 + 3\hat{S}_x x_{\rm X} y_{\rm X} + 3\hat{S}_y {y_{\rm X}}^2 + 3\hat{S}_z y_{\rm X} z_{\rm X}\right)\sin\Omega\right], \tag{19}$$

$$A_\tau^{\rm GM} = -\frac{GS_{\rm X}\csc I}{c^2 r_{\rm X}^5}\left\{\sin I\left[-3\left(\hat{S}_x x_{\rm X} + \hat{S}_y y_{\rm X}\right) z_{\rm X} + \hat{S}_z\left(r_{\rm X}^2 - 3{z_{\rm X}}^2\right)\right] + \right.$$

$$+ \cos I\left[\hat{S}_y\left(r_{\rm X}^2 - 3{y_{\rm X}}^2\right) - 3\left(\hat{S}_x x_{\rm X} + \hat{S}_z z_{\rm X}\right) y_{\rm X}\right]\cos\Omega +$$

$$\left. + \cos I\left[\hat{S}_x\left(-r_{\rm X}^2 + 3x_{\rm X}^2\right) + 3\hat{S}_y x_{\rm X} y_{\rm X} + 3\hat{S}_z x_{\rm X} z_{\rm X}\right]\sin\Omega\right\}, \tag{20}$$

$$A_\nu^{\rm GM} = \frac{GS_{\rm X}\csc I}{c^2 r_{\rm X}^5}\left\{\left[\hat{S}_y\left(r_{\rm X}^2 - 3{y_{\rm X}}^2\right) - 3y_{\rm X}\left(\hat{S}_x x_{\rm X} + \hat{S}_z z_{\rm X}\right)\right]\cos\Omega + \right.$$

$$\left. + \left[\hat{S}_x\left(-r_{\rm X}^2 + 3x_{\rm X}^2\right) + 3\hat{S}_y x_{\rm X} y_{\rm X} + 3\hat{S}_z x_{\rm X} z_{\rm X}\right]\sin\Omega\right\}. \tag{21}$$

They have to be inserted into the right-hand-sides of the standard Gauss equations for the variation of the orbital elements [4,10,16] which, finally, are doubly averaged with respect to $P_{\rm b}$, $P_{\rm b}^{\rm X}$ in the same way as previously described for the disturbing potential of Equation (1).

Even putting aside the post-Keplerian effects of classical and pN nature depending on the specific characteristics of the field of M itself, the motion of the test particle is perturbed also by the Newtonian 3-body acceleration due to the gravitational pull of X. By coupling with Equation (18), it would give rise to mixed orbital perturbations which can be worked out, in principle, as in Iorio [18], Will [19]. A rigorous calculation of such effects is outside the scope of the present paper. An approximate evaluation of their order of magnitude can be made as follows. For the sake

of simplicity, let the motion of $\mathcal{S}$ occur in a plane perpendicular to $\mathbf{S}_{\rm X}$, assumed as reference $\{x,\ y\}$ plane so that $I_{\rm X}=0,\ \hat{\mathbf{S}}_{\rm X}\cdot\hat{\boldsymbol{r}}_{\rm X}=0,\ \hat{S}_x=\hat{S}_y=0,\ \hat{S}_z=1$, along a circular orbit with $r/r_{\rm X}\ll 1$. Thus, the Newtonian 3-body acceleration felt by the test particle, obtainable from the tidal-type potential by Hogg, Quinlan & Tremaine [20], can be approximately posed equal to $\boldsymbol{A}_{\rm X}\simeq\left(GM_{\rm X}/r_{\rm X}^2\right)\hat{\boldsymbol{r}}_{\rm X}$ by neglecting the other two terms proportional to $(r/r_{\rm X})\,\hat{\boldsymbol{r}},\ (r/r_{\rm X})\,(\hat{\boldsymbol{r}}\cdot\hat{\boldsymbol{r}}_{\rm X})\,\hat{\boldsymbol{r}}_{\rm X}$. Then, following Iorio [18], it can be shown that the resulting mixed precessions are proportional to $\xi_{\rm X}\,(v_{\rm X}/c)^2\,(M_{\rm X}/M)\,(R_{\rm X}/r_{\rm X})^2\,(r/r_{\rm X})^2\,\Psi_{\rm X}$, where $v_{\rm X}\simeq\sqrt{GM_{\rm X}/r_{\rm X}}$ is the orbital velocity of $\mathcal{S}$ about X, and $\xi_{\rm X}<1,\ R_{\rm X},\ \Psi_{\rm X}$ are the normalized moment of inertia, the equatorial radius and the angular speed of X, respectively. This implies that the mixed effects are smaller than Equations (4)–(8) by a scaling factor of the order of $(M_{\rm X}/M)\,(r/r_{\rm X})^2$. In the case of, say, Jupiter and Europa, by assuming r approximately equal to the moon's radius R, it amounts to $\simeq$0.2.

We successfully checked our analytical results of Equations (4)–(11) as follows. We considered a fictitious system $\mathcal{S}$ orbiting a Jupiter-like body X along the same orbit of, say, Callisto, whose mass was assumed for the particle's primary M, and numerically integrated its equations of motion over a time span much longer than $P_{\rm b},\ P_{\rm b}^{X}$ with and without the pN gravitomagnetic acceleration of Equation (18) affecting the test particle; both the integrations, which assumed a purely Keplerian motion of $\mathcal{S}$ about the fictitious body X, shared the same initial conditions for the test particle and its primary. For X, the same physical properties of Jupiter were assumed, including the size and the orientation of its angular momentum $\mathbf{S}$. As a result, numerically produced times series of the orbital elements of the putative probe were produced by subtracting the purely classical ones from those obtained by including also Equation (18) in the equations of motion; they are displayed in Figure 1. It turned out that the resulting numerically calculated pN gravitomagnetic 3-body orbital shifts agree with those computed by means of the analytical formulas of Equations (4)–(11).

3. Some Potentially Interesting Astronomical Scenarios

In the case of a hypothetical orbiter of the Kronian natural satellite Enceladus in the external field of Saturn, Equations (6), (7), (9) and (10), referred to the mean Earth's equator at the reference epoch J2000.0 as reference $\{x,\ y\}$ plane, yield for a circular orbit ($e=0$), assumed just for the sake of simplicity,

$$\dot{I}=A_{\rm eq}\sin\left(\Omega+\varphi_{\rm eq}\right), \tag{22}$$

$$\dot{\Omega}=-49.9\ \text{mas year}^{-1}+\cot I\ A_{\rm eq}\cos\left(\Omega+\varphi_{\rm eq}\right), \tag{23}$$

with

$$A_{\rm eq}=-5.7\ \text{mas year}^{-1}, \tag{24}$$

$$\varphi_{\rm eq}=49.4\ \text{deg}. \tag{25}$$

Instead, if the mean ecliptic at the reference epoch J2000.0 is adopted as reference $\{x,\ y\}$ plane, we have

$$\dot{I}=A_{\rm ecl}\sin\left(\Omega+\varphi_{\rm ecl}\right), \tag{26}$$

$$\dot{\Omega}=-34.0\ \text{mas year}^{-1}+\cot I\ A_{\rm ecl}\cos\left(\Omega+\varphi_{\rm ecl}\right), \tag{27}$$

with

$$A_{\rm ecl}=23.9\ \text{mas year}^{-1}, \tag{28}$$

$$\varphi_{\rm ecl}=10.4\ \text{deg}. \tag{29}$$

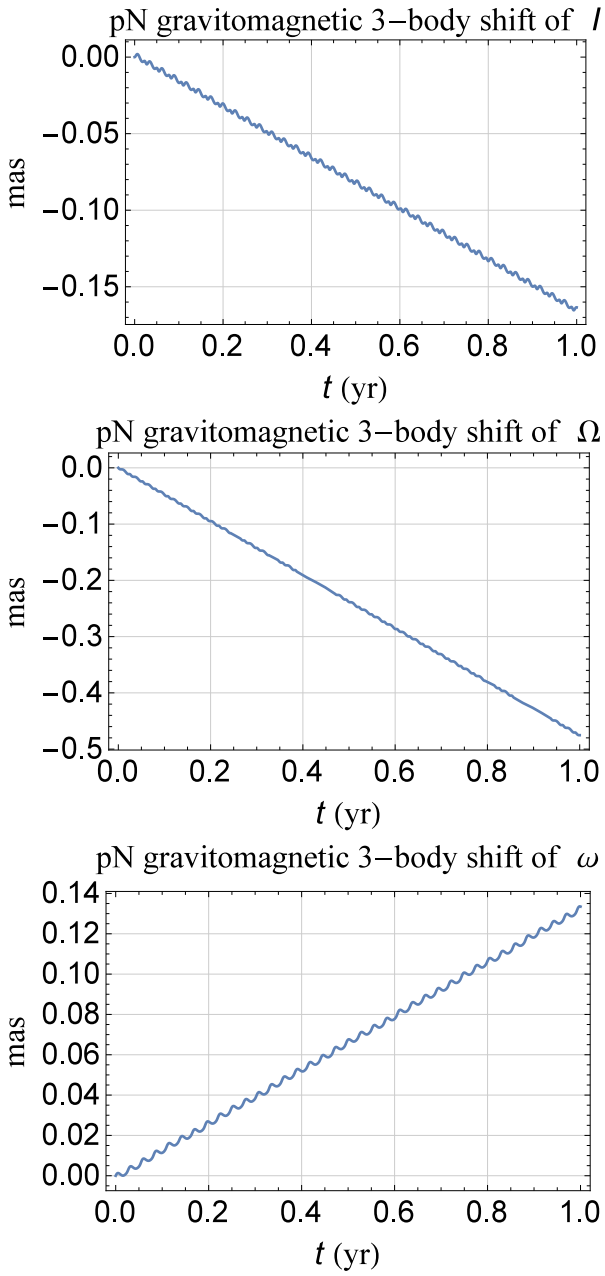


Figure 1. Numerical time series of the pN 3-body shifts of I, Ω, ω of a fictitious test particle moving around a Callisto-like primary M which orbits a Jupiter-type 3rd body X. They were obtained by integrating the equations of motion of the orbiter about M and of M about X in Cartesian rectangular coordinates referred to the Earth's mean equator at the epoch J2000.0 with and without Equation (18) acting on the test particle. Both runs shared the same set of arbitrary initial conditions for the probe $P_{\rm b} = 10.07$ d, $e_0 = 0.3$, $I_0 = 80$ deg, $\Omega_0 = 230$ deg, $\omega_0 = 40$ deg, $f_0 = 50$ deg and the primary; the initial state vector of the Callisto-Jupiter relative motion was adopted from the database JPL HORIZONS. For each Keplerian orbital element, its time series calculated from the purely Newtonian run was subtracted from that obtained from the pN integration in order to obtain the signatures displayed here. The resulting rates, in mas year^{-1}, agree with those computed in Equations (6)–(8).

By looking at a putative orbiter of the Jovian natural satellite Europa in the external field of Jupiter, we have

$$\dot{I} = A_{\rm eq} \sin\left(\Omega + \varphi_{\rm eq}\right), \tag{30}$$

$$\dot{\Omega} = -9.9 \text{ mas year}^{-1} + \cot I \, A_{\rm eq} \cos\left(\Omega + \varphi_{\rm eq}\right), \tag{31}$$

with

$$A_{\rm eq} = 4.8 \text{ mas year}^{-1}, \tag{32}$$

$$\varphi_{\rm eq} = 2.9 \text{ deg}, \tag{33}$$

and

$$\dot{I} = A_{\rm ecl} \sin\left(\Omega + \varphi_{\rm ecl}\right), \tag{34}$$

$$\dot{\Omega} = -11.0 \text{ mas year}^{-1} + \cot I \, A_{\rm ecl} \cos\left(\Omega + \varphi_{\rm ecl}\right), \tag{35}$$

with

$$A_{\rm ecl} = 0.3 \text{ mas year}^{-1}, \tag{36}$$

$$\varphi_{\rm ecl} = 31.0 \text{ deg}. \tag{37}$$

We considered just Enceladus and Europa because they are of great planetological interest in view of the possible habitability of their oceans beneath their icy crusts [21]. As a consequence, they are the natural targets of several concept studies and proposals for dedicated missions to them, including also orbiters [22–26]. Since, at present, sending a spacecraft to Europa seems more likely than to Enceladus, as it can be learnt at https://europa.nasa.gov/about-clipper/overview/ and http://sci.esa.int/juice/ on the Internet, we investigated in a little more detail this potentially appealing Jovian scenario, even if it is not said that the actually approved missions will finally involve the use of an orbiter. In such kind of endeavours, the observable quantity is typically the Earth-probe range-rate $\dot{\rho}$, whose accuracy for, e.g., the ongoing mission Juno [27] around Jupiter is $\sigma_{\dot{\rho}} \simeq 0.015$ mm s^{-1} [28]. Figure 2 shows the numerically simulated Earth-spacecraft range-rate signature due to the pN gravitomagnetic 3-body acceleration of Equation (18) for a generic orbital configuration of the hypothesized orbiter. To produce it, we numerically integrated the equations of motion in Cartesian rectangular coordinates of the Earth, Jupiter, its Galilean moons and a fictitious test particle orbiting Europa over 1 d. In both runs, sharing the same initial conditions retrieved from the database JPL HORIZONS (https://ssd.jpl.nasa.gov/?horizons) at the arbitrary epoch of midnight on 1 January 2030, we modeled the mutual attractions among all the bodies involved to the Newtonian level, with the exception of Equation (18) which was added to the other classical gravitational pulls felt by the probe in one of the runs. Then, we numerically calculated two range-rate time series, with and without Equation (18) *ceteris paribus*, and subtracted the purely Newtonian one from that including also the pN gravitomagnetic acceleration. It can be noted that, for the orbital configuration chosen, the range-rate relativistic signature $\Delta\dot{\rho}$ reaches the 0.05 mm s^{-1} level after just 1 d. Thus, the scenario considered seems worthy of further, dedicated analyses investigating the actual measurability of Equation (18) in a realistic error budget analysis and mission proposal. It should take into account several concurring perturbations of gravitational and non-gravitational nature, and also several technological and engineering issues.

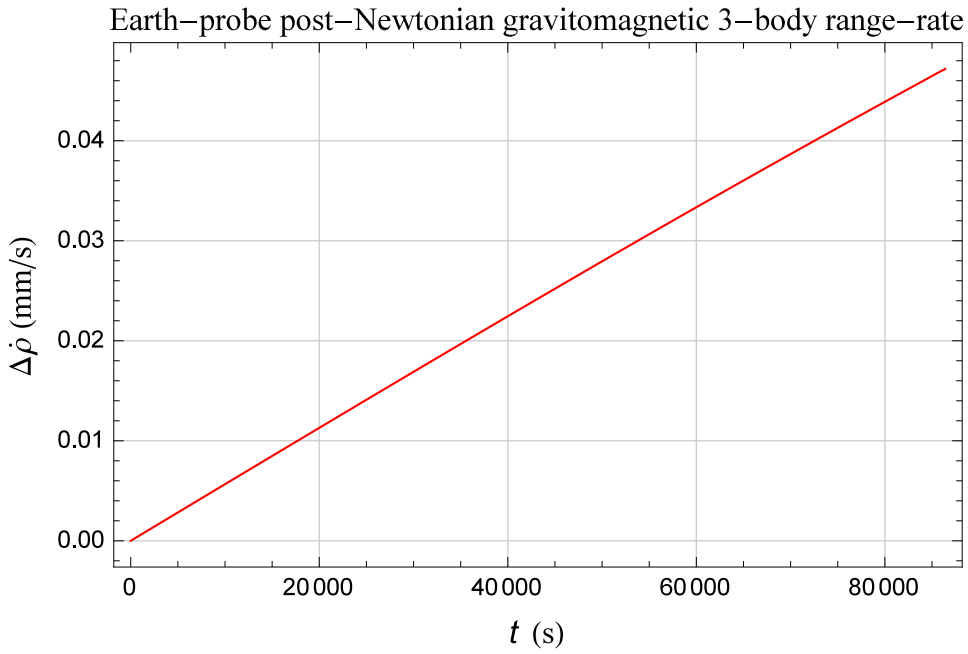


Figure 2. Numerically produced Earth-probe range-rate shift $\Delta\dot{\rho}\,(t)$ due to the pN gravitomagnetic 3-body acceleration of Equation (18). We numerically integrated the solar system barycentric equations of motion in Cartesian rectangular coordinates of the Earth, Jupiter, its Galilean moons and a fictitious test particle orbiting Europa over 1 d. In both runs, sharing the same initial conditions for all the existing natural bodies retrieved from the database JPL HORIZONS (https://ssd.jpl.nasa.gov/?horizons) at the arbitrary epoch of midnight of 1 January 2030, we modeled the mutual attractions among all the planets and the satellites involved to the Newtonian level, with the exception of Equation (18) which was added to the other classical gravitational pulls felt by the orbiter in one of the runs. Then, we numerically calculated two range-rate time series, and subtracted the purely Newtonian one from that including also Equation (18). The orbital configuration adopted for the spacecraft, referred to Europa, was $a_0 = 3.55\,R$, $e_0 = 0.69$, $I_0 = 100$ deg, $\Omega_0 = 90$ deg, $\omega_0 = 40$ deg, $f_0 = 50$ deg, where R is the radius of Jovian moon.

In the case of an artificial satellite orbiting a planet in the field of the Sun, the effects are much smaller. For an Earth's spacecraft in a circular orbit, we have

$$\dot{I} = A_{\rm eq}\sin\left(\Omega + \varphi_{\rm eq}\right), \tag{38}$$

$$\dot{\Omega} = -0.2\,\mu\text{as year}^{-1} + \cot I\, A_{\rm eq}\cos\left(\Omega + \varphi_{\rm eq}\right), \tag{39}$$

with

$$A_{\rm eq} = 0.1\,\mu\text{as year}^{-1}, \tag{40}$$

$$\varphi_{\rm eq} = 9.13\,\text{deg}, \tag{41}$$

and

$$\dot{I} = A_{\rm ecl}\sin\left(\Omega + \varphi_{\rm ecl}\right), \tag{42}$$

$$\dot{\Omega} = -0.3\,\mu\text{as year}^{-1} + \cot I\, A_{\rm ecl}\cos\left(\Omega + \varphi_{\rm ecl}\right), \tag{43}$$

with

$$A_{\rm ecl} = 0.02\ \mu\text{as year}^{-1}, \tag{44}$$

$$\varphi_{\rm ecl} = 104.2\ \text{deg}. \tag{45}$$

For a probe orbiting Mercury with $e = 0$, one gets

$$\dot{I} = A_{\rm eq}\sin\left(\Omega + \varphi_{\rm eq}\right), \tag{46}$$

$$\dot{\Omega} = -4.3\ \mu\text{as year}^{-1} + \cot I\ A_{\rm eq}\cos\left(\Omega + \varphi_{\rm eq}\right), \tag{47}$$

with

$$A_{\rm eq} = -2.5\ \mu\text{as year}^{-1}, \tag{48}$$

$$\varphi_{\rm eq} = 171.3\ \text{deg}, \tag{49}$$

and

$$\dot{I} = A_{\rm ecl}\sin\left(\Omega + \varphi_{\rm ecl}\right), \tag{50}$$

$$\dot{\Omega} = -5\ \mu\text{as year}^{-1} + \cot I\ A_{\rm ecl}\cos\left(\Omega + \varphi_{\rm ecl}\right), \tag{51}$$

with

$$A_{\rm ecl} = -0.6\ \mu\text{as year}^{-1}, \tag{52}$$

$$\varphi_{\rm ecl} = 144.6\ \text{deg}. \tag{53}$$

4. Summary and Overview

In the weak-field and slow-motion approximation of general relativity, we analytically worked out the pN gravitomagnetic long-term rates of change of the relevant Keplerian orbital elements of a test particle orbiting a primary M at distance r from it which, in turn, moves in the external spacetime deformed by the mass-energy currents of the spin angular momentum $\boldsymbol{S}_{\rm X}$ of a distant ($r_{\rm X} \gg r$) 3rd body X with mass $M_{\rm X} \gg M$. We did not assume any preferred orientation for the spin axis $\hat{\boldsymbol{S}}_{\rm X}$ of the external body; moreover, we did not make simplifying assumptions pertaining the orbital configurations of both the M's satellite and of M itself in its motion around $M_{\rm X}$. Thus, our calculation has a general validity, being applicable to arbitrary astronomical systems of potential interest. It turns out that, by doubly averaging the perturbing potential employed in the calculation with respect to the orbital periods $P_{\rm b}$, $P_{\rm b}^{\rm X}$ of both M and $M_{\rm X}$, the semimajor axis a and the eccentricity e do not experience long-term variations, contrary to the inclination I of the orbital plane, the longitude of the ascending node Ω and the argument of pericenter ω. While the gravitomagnetic rates $\dot{I}$ and $\dot{\omega}$ are harmonic signatures characterized by the frequency of the possible variation of the node Ω, induced by other dominant perturbations like, e.g., the Newtonian quadrupole mass moment of the satellite's primary M, the gravitomagnetic node rate $\dot{\Omega}$ exhibits also a secular trend in addition to a harmonic component with the frequency of the node itself. A numerical integration of the equations of motion of a fictitious 3-body system made of a distant spinning body with the same physical properties of Jupiter, a primary with the same orbital and physical characteristics of Callisto and a test particle orbiting it confirms our analytical results.

The Sun's angular momentum exerts very small effects on spacecraft orbiting Mercury ($\simeq 1\ \mu\text{as year}^{-1}$) and the Earth ($\sim 0.1\ \mu\text{as year}^{-1}$). Instead, the angular momenta of the gaseous giant planets like Jupiter and Saturn may induce much larger perturbations of the orbital motions of hypothetical anthropogenic orbiters of some of their major natural moons like, e.g., Europa ($\lesssim$10 mas year^{-1}) and Enceladus ($\lesssim$50 mas year^{-1}). Such natural satellites have preeminent interest

in planetology, making them ideal targets for future, dedicated spacecraft-based missions which may be opportunistically exploited to attempt to measure such relativistic effects as well. In the case of Europa, for whose exploration there are already approved missions by NASA and ESA, a preliminary numerical simulation of the signature induced by the pN gravitomagnetic 3-body effect of interest on the range-rate of a putative orbiter shows that, for certain orbital configurations, its magnitude can become larger than the present-day accuracy $\sigma_{\dot{\rho}} = 0.015$ mm s^{-1} of the current Juno mission around Jupiter after 1 d.

Acknowledgments: I thank M. Efroimsky for his useful remarks which contributed to improve the manuscript.

Conflicts of Interest: The authors declare no conflict of interest.

Appendix A. Notations and Definitions

Here, some basic notations and definitions pertaining the restricted two-body system $\mathcal{S}$ moving in the external field of the distant 3rd body X considered in the text are presented. For the numerical values of some of them, see Tables A1 and A2.

G : Newtonian constant of gravitation
c : speed of light in vacuum
ϵ : mean obliquity
$M_{\rm X}$: mass of the distant 3rd body X (a star like the Sun or a planet like, e.g., Jupiter or Saturn)
$\mu_{\rm X} \doteq GM_{\rm X}$: gravitational parameter of the 3rd body X
$R_{\rm X}$: equatorial radius of the 3rd body X
$S_{\rm X}$: magnitude of the angular momentum of the 3rd body X
$\zeta_{\rm X}$: normalized moment of inertia of the 3rd body X
$\Psi_{\rm X}$: angular speed of the 3rd body X
$\hat{\mathbf{S}}_{\rm X} = \{\hat{S}_x,\ \hat{S}_y,\ \hat{S}_z\}$: spin axis of the 3rd body X in some coordinate system
$\alpha_{\rm X}$: right ascension (RA) of the 3rd body's spin axis
$\delta_{\rm X}$: declination (DEC) of the 3rd body's spin axis
$\hat{S}_x^{\rm eq} = \cos\delta_{\rm X}\cos\alpha_{\rm X}$: component of the 3rd body's spin axis w.r.t. the reference x axis of an equatorial coordinate system
$\hat{S}_y^{\rm eq} = \cos\delta_{\rm X}\sin\alpha_{\rm X}$: component of the 3rd body's spin axis w.r.t. the reference y axis of an equatorial coordinate system
$\hat{S}_z^{\rm eq} = \sin\delta_{\rm X}$: component of the 3rd body's spin axis w.r.t. the reference z axis of an equatorial coordinate system
$\boldsymbol{r}_{\rm X}$: position vector towards the 3rd body X
$r_{\rm X}$: distance of $\mathcal{S}$ to the 3rd body X
$\hat{\boldsymbol{r}}_{\rm X} \doteq \boldsymbol{r}_{\rm X}/r_{\rm X}$: versor of the position vector towards the 3rd body X
$a_{\rm X}$: semimajor axis of the orbit about the 3rd body X
$n_{\rm b}^{\rm X} \doteq \sqrt{\mu_{\rm X}/a_{\rm X}^3}$: mean motion of the orbit about the 3rd body X
$P_{\rm b}^{\rm X} \doteq 2\pi/n_{\rm b}^{\rm X}$: orbital period of the orbit about the 3rd body X
$e_{\rm X}$: eccentricity of the orbit about the 3rd body X
$I_{\rm X}$: inclination of the orbital plane of orbit about the 3rd body X to the reference $\{x,\ y\}$ plane of some coordinate system
$\Omega_{\rm X}$: longitude of the ascending node of the orbit about the 3rd body X referred to the reference $\{x,\ y\}$ plane of some coordinate system
M : mass of the primary (planet or planetary natural satellite) orbited by the test particle and moving in the external field of the 3rd body X

$\mu \doteq GM$: gravitational parameter of the primary orbited by the test particle and moving in the external field of the 3rd body X
R : radius of the primary (planet or planetary natural satellite) orbited by the test particle and moving in the external field of the 3rd body X
$\boldsymbol{S}$: angular momentum of the primary
$\boldsymbol{r}$: position vector of the test particle with respect to its primary
r : magnitude of the position vector of the test particle
$\boldsymbol{v}$: velocity vector of the test particle
$\boldsymbol{L} \doteq \boldsymbol{r} \times \boldsymbol{v}$: orbital angular momentum per unit mass of the test particle
a : semimajor axis of the test particle's orbit
$n_{\mathrm{b}} \doteq \sqrt{\mu/a^3}$: Keplerian mean motion of the test particle's orbit
$P_{\mathrm{b}} \doteq 2\pi/n_{\mathrm{b}}$: orbital period of the test particle's orbit
e : eccentricity of the test particle's orbit
f : true anomaly of the test particle's orbit
I : inclination of the orbital plane of the test particle's orbit to the reference $\{x, y\}$ plane of some coordinate system
Ω : longitude of the ascending node of the test particle's orbit referred to the reference $\{x, y\}$ plane of some coordinate system

Appendix B. Tables

Table A1. Relevant physical and orbital parameters for Saturn, Jupiter, Enceladus and Europa. Most of the reported values come from Petit, Luzum & et al. [29], Seidelmann et al. [30], Soffel et al. [31] and references therein. The source for the orbital elements referred to either the mean ecliptic (ecl) at the reference epoch J2000.0 or the mean Earth's equator (eq) at the same epoch is the freely consultable database JPL HORIZONS on the Internet at https://ssd.jpl.nasa.gov/?horizons from which they were retrieved by choosing the time of writing this paper as input epoch.

Parameter	Units	Numerical Value
G	$\mathrm{kg}^{-1}\,\mathrm{kgm}^3\,\mathrm{s}^{-2}$	6.67259×10^{-11}
c	$\mathrm{m\,s}^{-1}$	2.99792458×10^{8}
$S_{\mathfrak{h}}$	$\mathrm{kg\,m}^2\,\mathrm{s}^{-1}$	1.4×10^{38}
$\alpha_{\mathfrak{h}}$	deg	40.59
$\delta_{\mathfrak{h}}$	deg	83.54
a_{Enc}	km	237,948
e_{Enc}	–	0.0047
$I^{\mathrm{eq}}_{\mathrm{Enc}}$	deg	6.475336858877378
$I^{\mathrm{ecl}}_{\mathrm{Enc}}$	deg	28.06170970578348
$\Omega^{\mathrm{eq}}_{\mathrm{Enc}}$	deg	130.5900992493321
$\Omega^{\mathrm{ecl}}_{\mathrm{Enc}}$	deg	169.5108697290241
$P^{\mathrm{Enc}}_{\mathrm{b}}$	d	1.370218
$S_{\mathfrak{4}}$	$\mathrm{kg\,m}^2\,\mathrm{s}^{-1}$	6.9×10^{38}
$\alpha_{\mathfrak{4}}$	deg	268.05
$\delta_{\mathfrak{4}}$	deg	64.49
a_{Eur}	km	671,034
e_{Eur}	–	0.0094
$I^{\mathrm{eq}}_{\mathrm{Eur}}$	deg	25.88280598312641
$I^{\mathrm{ecl}}_{\mathrm{Eur}}$	deg	1.790876103183550
$\Omega^{\mathrm{eq}}_{\mathrm{Eur}}$	deg	357.4169659423443
$\Omega^{\mathrm{ecl}}_{\mathrm{Eur}}$	deg	332.6268549691798
$P^{\mathrm{Eur}}_{\mathrm{b}}$	d	3.551810

Table A2. Relevant physical and orbital parameters used in the text for the Sun, Mercury and the Earth. Most of the reported values come from Petit, Luzum & et al. [29], Seidelmann et al. [30], Soffel et al. [31] and references therein. The source for the orbital elements referred to either the mean ecliptic (ecl) at the reference epoch J2000.0 or the mean Earth's equator (eq) at the same epoch is the freely consultable database JPL HORIZONS on the Internet at https://ssd.jpl.nasa.gov/?horizons from which they were retrieved by choosing the time of writing this paper as input epoch.

Parameter	Units	Numerical Value
G	$\mathrm{kg}^{-1}\,\mathrm{m}^3\,\mathrm{s}^{-2}$	6.67259×10^{-11}
c	$\mathrm{m\,s}^{-1}$	2.99792458×10^{8}
$S_\odot$	$\mathrm{kg\,m}^2\,\mathrm{s}^{-1}$	1.90×10^{41}
$\alpha_\odot$	deg	286.13
$\delta_\odot$	deg	63.87
$a_{\mercury}$	au	0.3870982252717257
$e_{\mercury}$	–	0.2056302512089075
$I^{\mathrm{eq}}_{\mercury}$	deg	28.55225598038233
$I^{\mathrm{ecl}}_{\mercury}$	deg	7.005014199657344
$\Omega^{\mathrm{eq}}_{\mercury}$	deg	10.98794759075666
$\Omega^{\mathrm{ecl}}_{\mercury}$	deg	48.33053756455964
$P^{\mercury}_{\mathrm{b}}$	yr	0.2408467
$a_\oplus$	au	0.9992521882390240
$e_\oplus$	–	0.01731885059206812
$I^{\mathrm{eq}}_\oplus$	deg	23.43903457134406
$I^{\mathrm{ecl}}_\oplus$	deg	$2.669113820737183 \times 10^{-4}$
$\Omega^{\mathrm{eq}}_\oplus$	deg	$1.852352676284691 \times 10^{-4}$
$\Omega^{\mathrm{ecl}}_\oplus$	deg	163.9752443600624
$P^{\oplus}_{\mathrm{b}}$	yr	1.0000174

References

1. Frutos-Alfaro, F.; Soffel, M. On relativistic multipole moments of stationary space-times. *R. Soc. Open Sci.* **2018**, *5*, 180640. [CrossRef] [PubMed]
2. Soffel, M.; Frutos, F. On the Usefulness of Relativistic Space-Times for the Description of the Earth's Gravitational Field. *J. Geod.* **2016**, *90*, 1345–1357. [CrossRef]
3. Capderou, M. *Satellites: Orbits and Missions*; Springer: Berlin, Germany, 2005.
4. Poisson, E.; Will, C.M. *Gravity*; Cambridge University Press: Cambridge, UK, 2014.
5. Angélil, R.; Saha, P.; Bondarescu, R.; Jetzer, P.; Schärer, A.; Lundgren, A. Spacecraft clocks and relativity: Prospects for future satellite missions. *Phys. Rev. D* **2014**, *89*, 064067. [CrossRef]
6. Schanner, M.; Soffel, M. Relativistic satellite orbits: Central body with higher zonal harmonics. *Celest. Mech. Dyn. Astr.* **2018**, *130*, 40. [CrossRef]
7. Schärer, A.; Bondarescu, R.; Saha, P.; Angélil, R.; Helled, R.; Jetzer, P. Prospects for Measuring Planetary Spin and Frame-Dragging in Spacecraft Timing Signals. *Front. Astron. Space Sci.* **2017**, *4*, 11. [CrossRef]
8. Brumberg, V.A.; Kopeikin, S.M. Relativistic reference systems and motion of test bodies in the vicinity of the Earth. *Nuovo Cimento B* **1989**, *103*, 63–98. [CrossRef]
9. Damour, T.; Soffel, M.; Xu, C. General-relativistic celestial mechanics. IV. Theory of satellite motion. *Phys. Rev. D* **1994**, *49*, 618. [CrossRef]
10. Kopeikin, S.; Efroimsky, M.; Kaplan, G. *Relativistic Celestial Mechanics of the Solar System*; Wiley-VCH: Weinheim, Germany, 2011.
11. de Sitter, W. Einstein's theory of gravitation and its astronomical consequences, Second Paper. *Mon. Not. R. Astron. Soc.* **1916**, *77*, 155–184. [CrossRef]

12. Fokker, A.D. De geodetische precessie; een uitvloeisel van Einstein's gravitatie- theorie. *Versl. Kon. Ak. Wet.* **1920**, *29*, 611–621.
13. Schouten, W.J.A. Over het ontstaan eener praecessiebeweging tengevolge van het niet euklidisch zijn der ruimte in de nabijheiud van zon. *Versl. Kon. Ak. Wet.* **1918**, *27*, 214.
14. Gill, E.; Soffel, M.; Ruder, H.; Schneider, M. *Relativistic Motion of Gyroscopes and Space Gradiometry*; Deutsche Geodätische Kommission: München, Germany, 1992.
15. Barker, B.M.; O'Connell, R.F. The gravitational interaction: Spin, rotation, and quantum effects-A review. *Gen. Relat. Gravit.* **1979**, *11*, 149–175. [CrossRef]
16. Bertotti, B.; Farinella, P.; Vokrouhlický, D. *Physics of the Solar System*; Kluwer Academic Press: Dordrecht, The Netherlands, 2003.
17. Efroimsky, M. Gauge freedom in orbital mechanics. *Ann. N. Y. Acad. Sci.* **2005**, *1065*, 346–374. [CrossRef]
18. Iorio, L. Post-Newtonian direct and mixed orbital effects due to the oblateness of the central body. *Int. J. Mod. Phys. D* **2015**, *24*, 1550067. [CrossRef]
19. Will, C.M. Incorporating post-Newtonian effects in N-body dynamics. *Phys. Rev. D* **2014**, *89*, 044043. [CrossRef]
20. Hogg, D.W.; Quinlan, G.D.; Tremaine, S. Dynamical limits on dark mass in the outer solar system. *Astron. J.* **1991**, *101*, 2274–2286. [CrossRef]
21. Lunine, J.I. Ocean worlds exploration. *Acta Astronaut.* **2017**, *131*, 123–130. [CrossRef]
22. MacKenzie, S.M.; Caswell, T.E.; Phillips-Lander, C.M.; Stavros, E.N.; Hofgartner, J.D.; Sun, V.Z.; Powell, K.E.; Steuer, C.J.; O'Rourke, J.G.; Dhaliwal, J.K.; et al. THEO concept mission: Testing the habitability of Enceladus's Ocean. *Adv. Space Res.* **2016**, *58*, 1117–1137. [CrossRef]
23. Razzaghi, A.I.; di Pietro, D.A.; Quinn, D.A.; Simon-Miller, A.A.; Tompkins, S.D. *Space Technology and Applications International Forum-STAIF 2008*; American Institute of Physics Conference Series; El-Genk, M.S., Ed.; American Institute of Physics: College Park, MD, USA, 2008; Volume 969, pp. 388–395.
24. Sherwood, B.; Lunine, J.; Sotin, C.; Cwik, T.; Naderi, F. Program options to explore ocean worlds. *Acta Astronaut.* **2018**, *143*, 285–296. [CrossRef]
25. Spencer, J.; Niebur, C. *Planetary Science Decadal Survey. Enceladus Orbiter*; National Aeronautics and Space Administration: Washington, DC, USA, 2010.
26. Verma, A.K.; Margot, J.-L. Expected precision of Europa Clipper gravity measurements. *Icarus* **2018**, *314*, 35–49. [CrossRef]
27. Bolton, S.J.; Lunine, J.; Stevenson, D.; Connerney, J.E.P.; Levin, S.; Owen, T.C.; Bagenal, F.; Gautier, D.; Ingersoll, A.P.; Orton, G.S.; et al. The Juno mission. *Space Sci. Rev.* **2017**, *213*, 5–37. [CrossRef]
28. Iess, L.; Folkner, W.M.; Durante, D.; Parisi, M.; Kaspi, Y.; Galanti, E.; Guillot, T.; Hubbard, W.B.; Stevenson, D.J.; Anderson, J.D.; et al. Measurement of Jupiter's asymmetric gravity field. *Nature* **2018**, *555*, 220–222. [CrossRef] [PubMed]
29. Petit, G.; Luzum, B. IERS Conventions. *IERS Tech. Note* **2010**, *36*, 1.
30. Seidelmann, P.K.; Archinal, B.A.; A'hearn, M.F.; Conrad, A.; Consolmagno, G.J.; Hestroffer, D.; Hilton, J.L.; Krasinsky, G.A.; Neumann, G.; Oberst, J.; et al. Report of the IAU/IAG Working Group on cartographic coordinates and rotational elements: 2006. *Celest. Mech. Dyn. Astr.* **2007**, *98*, 155–180. [CrossRef]
31. Soffel, M.; Klioner, S.A.; Petit, G.; Wolf, P.; Kopeikin, S.M.; Bretagnon, P.; Brumberg, V.A.; Capitaine, N.; Damour, T.; Fukushima, T.; et al. The IAU 2000 resolutions for astrometry, celestial mechanics, and metrology in the relativistic framework: Explanatory supplement. *Astron. J.* **2003**, *126*, 2687. [CrossRef]



© 2019 by the author. Licensee MDPI, Basel, Switzerland. This article is an open access article distributed under the terms and conditions of the Creative Commons Attribution (CC BY) license (http://creativecommons.org/licenses/by/4.0/).